Proceedings of the Twenty-seventh (2017) International Ocean and Polar Engineering Conference **www.isope.org**
San Francisco, CA, USA, June 25-30, 2017

ISBN 978-1-880653-97-5; ISSN 1098-6189

A Hybrid Solver Based on Efficient BEM-potential and LBM-NS Models: Recent LBM Developments and Applications to Naval Hydrodynamics

C.M. O'Reilly[1,2], *S.T. Grilli*[1], *J.C. Harris*[3], *A. Mivehchi*[1], *C.F. Janssen*[4], *J.M. Dahl*[1]
(1) Dept. of Ocean Engineering, University of Rhode Island, Narragansett, RI, USA
(2) Navatek Ltd., South Kingstown, RI, USA
(3) LHSV, Ecole des Ponts, CEREMA, EDF R&D, Université Paris-Est, Chatou, France
(4) Fluid Dynamics and Ship Theory Inst., Hamburg University of Technology (TUHH), Germany

ABSTRACT

We report on recent progress and validation of a 3D hybrid model for naval hydrodynamics problems based on a perturbation method, in which both velocity and pressure are expressed as the sum of an inviscid flow with a viscous perturbation. The far- to near-field inviscid flows can be solved with a Boundary Element Method (BEM), based on fully nonlinear potential flow theory, and the near-field perturbation flow is solved with a NS model based on a Lattice Boltzmann Method (LBM) with a Large Eddy Simulation (LES) of the turbulence. We summarize the hybrid model formulation and latest developments regarding the LES, and particularly a new wall model for the viscous/turbulent sub-layer near solid boundaries, that is generalized for an arbitrary geometry. The latter are validated by simulating turbulent flows over a flat plate for Re $\in [3.7\times10^4; 1.2\times10^6]$, for which the friction coefficient computed on the plate agrees well with experiments. We then simulate the flow past a NACA0012 foil using the hybrid LBM-LES with the wall model, for Re $= 1\times10^6$, and show a good agreement of lift and drag forces with experiments. Results obtained with the hybrid LBM model are either nearly identical or improved relative to those of the standard LBM, but for a smaller computational domain, demonstrating the benefits of the hybrid approach.

INTRODUCTION

The simulation of large ship motions and resistance in steep waves is typically performed using linear or (more rarely) nonlinear potential flow solvers, usually based on a higher-order Boundary Element Method (BEM), with semi-empirical corrections introduced to account for viscous/turbulent effects. However in some cases, viscous/turbulent flows near the ship's hull, and breaking waves and wakes must be accurately modeled to capture the salient physics. Navier-Stokes (NS) solvers can and have been used to model such flows, but they are computationally expensive and often too numerically dissipative to model wave propagation over long distances.

Here, we detail the development of a 3D hybrid model, for solving naval hydrodynamics problems, based on a perturbation method (e.g., Alessandrini, 2007; Grilli, 2008; Harris and Grilli, 2012; O'Reilly et al. 2016), in which both velocity and pressure are expressed as the sum of an inviscid (I) and a viscous perturbation (P) component. In this model, the far- to near-field inviscid flow is solved with a BEM, based on fully nonlinear potential flow (FNPF) theory, also referred to as Numerical Wave Tank (NWT), and the near-field perturbation flow is solved with a NS model, here implemented with a Lattice Boltzmann Method (LBM; e.g., d'Humieres et al., 2002; Janssen, 2010; Janssen et al., 2010) including a Large Eddy Simulation of the turbulence (LES; e.g., Krafczyk et al., 2003). Both the BEM and LBM models have separate representations of the free surface (using an explicit Eulerian-Lagrangian time updating in the former and a VOF method in the latter; e.g., O'Reilly et al., 2015).

In the context of the hybrid perturbation method, the LBM is only applied to the near-field where viscous/turbulent effects matter, and its solution is forced by results of the NWT applied to the entire domain. Hence the hybrid approach has an increased computational efficiency relative to traditional CFD solutions, in which the NS solver is applied to the entire domain. This was already demonstrated by Reliquet et al. (2014) based on different types of models, which were not as efficient and optimized than those proposed here. Indeed, the NWT used here was the object of numerous developments over the past two decades (see Grilli et al.'s, 2010 review to date). Its latest version was optimized with a Fast Multipole Method (FMM), based on the parallel ExaFMM library, and shown to achieve nearly linear scaling on very large CPU clusters (e.g., Harris et al., 2014, Harris et al., 2016, and Mivehchi et al., in this conference). The LBM has proved to be accurate and efficient for simulating a variety of complex fluid flow and fluid-structure interaction problems and, when implemented on a massively parallel General Purpose Graphical Processor Unit (GPGPU) co-processor, it was also shown to achieve very high efficiency (over 100 million node updates per second on a single GPGPU of an older 2010-2012 generation than used nowadays; e.g., Janssen, 2010; Janssen et al., 2013; Banari et al., 2014). In this respect, LBM developments in this work are based on the highly efficient, GPGPU-accelerated, Lattice Boltzmann solver ELBE (Janssen et al., 2015; www.tuhh.de/elbe), developed at TUHH, which features various LBM models, an on-device grid generator, higher-order boundary conditions, and the possibility of specifying overlapping nested grids. ELBE also includes the initial LBM perturbation model based on Janssen et al.'s (2010) approach (discussed later). Simple validations of the hybrid LBM and LBM-LES approaches, for viscous and turbulent oscillatory boundary layers and turbulent channels, were reported by O'Reilly et al. (2015), O'Reilly et al. (2016), and Janssen et al. (2017).

In this paper, we focus on the development and validation of the hybrid NS-LBM solver applied to the perturbation flow and, in this context, on

the modeling of turbulent flows by a LES with a wall model. The latter allows for a more accurate representation of boundary layers near solid boundaries without the need for a refined discretization. The turbulent wall model formulation in our LBM model is an extension of the method originally proposed by Malaspinas and Sagaut (2014), in which we more accurately represent the geometry of wall boundaries of arbitrary shape and orientation.

We first summarize the principles of the LBM in the context of the Multiple Relaxation Time (MRT) method. We then detail the formulation of the perturbation method in the context of turbulent flows and show how the standard LES equations are modified. We then validate the hybrid LBM-LES approach by solving turbulent flows past a plane solid boundary, for which we both retrieve the "law of the wall" velocity profile and accurately compute the experimentally measured drag force. Finally, the method is validated in a more rigorous test, by computing the drag and lift coefficients of a submerged hydrofoil at a high Reynolds number $\mathrm{Re} = 1 \times 10^6$. It should be pointed out that this paper extends the work reported in O'Reilly et al. (2016), particularly regarding improvements of the turbulent wall model formulation when applied to complex geometries, which are validated with the hydrofoil simulations.

METHODOLOGY

Lattice Boltzmann Method (LBM)

In the LBM, the macroscopic NS equations are modeled by solving an equivalent mesoscopic problem in which the fluid is represented by particles interacting over a (typically regular) lattice (or grid), through their distribution functions (DF) $f(t,\mathbf{x},\xi)$, representing the normalized probability to find a particle at location $\mathbf{x}$ at time t with velocity ξ; the macroscopic hydrodynamic quantities (e.g., velocity, pressure,...) are defined as moments of the DFs.

The time evolution of discrete particle DFs is governed by the Boltzmann advection-collision equation,

$$\frac{Df_\alpha}{Dt} = \frac{\partial f_\alpha(t,\mathbf{x})}{\partial t} + \mathbf{e}_\alpha \cdot \frac{\partial f_\alpha(t,\mathbf{x})}{\partial \mathbf{x}} = \Omega_\alpha + B'_\alpha \tag{1}$$

in which $\mathbf{e}_\alpha$ denotes discrete particle velocities, Ω_α is a collision operator describing interactions between particles, and B'_α represents volume forces such gravity.

When discretizing Eq. (1) it is convenient to scale each parameter such that the mesh Courant number is unity and the particles move from lattice node to lattice node, thus eliminating the need for finite differencing between lattice nodes. We hereafter denote dimensional quantities by prime variables will while non-prime variables represent non-dimensional quantities, in which lengths have been divided by a length scale λ, times by time scale τ, and masses by mass scale ϖ; thus the particle propagation speed is $c = c'\tau/\lambda = \Delta x'/\Delta t'$, and a mesh Courant number of 1 yields $c = 1$. In LBM, one also typical assumes, $\lambda = \Delta x'$, thus $\Delta x = 1 \rightarrow \Delta t = 1$; finally the nondimensional viscosity reads, $\nu = \nu'\tau/\lambda^2$. In LBM simulations of flows at specified Mach and Reynolds numbers (Ma, Re), one thus finds, $\nu = c_s \ell \mathrm{Ma}/\mathrm{Re}$, to use in simulations, also given the physical length scale of the flow ℓ and speed of sound $c_s = c/\sqrt{3}$. This dimensional scaling has been applied to all variables for the remainder of this paper unless denoted with a prime.

Eq. (1) is discretized over a regular lattice, of grid spacing Δx using $n = 19$ discrete particle velocities, which point in the directions of 18 neighboring particles from a given particle location; thus: $\mathbf{e}_\alpha = \{0,0,0\};\{\pm c,0,0\};\{0,\pm c,0\};\{0,0,\pm c\};\{\pm c,\pm c,0\};\{\pm c,0,\pm c\};$ $\{0,\pm c,\pm c\}$, for $\alpha = 0,...,18$ (standard D3Q19 scheme).

In the standard Single Relaxation Time (SRT) LBM, Eq. (1) is discretized by finite differences in space and time as,

$$f_\alpha(t+\Delta t,\mathbf{x}+\mathbf{e}_\alpha\Delta t) - f_\alpha(t,\mathbf{x}) = -\frac{\Delta t}{\tau}\{f_\alpha(\mathbf{x},t) - f_\alpha^{eq}(\rho,\mathbf{u})\} + B_\alpha \tag{2}$$

where $f_\alpha^{eq}(\rho,\mathbf{u})$ are equilibrium DFs, functions of the macroscopic fluid density ρ and velocity $\mathbf{u}$, Δt is time step (with $c = \Delta x/\Delta t$), and τ, a nondimensional relaxation time (SRT). LBM simulations are typically split up into a *collision* step, which locally drives the particle DFs to equilibrium, and a *propagation* step, during which the evolved DFs are advected. The macroscopic hydrodynamic quantities are then found as low-order moments of the DFs, e.g.,

$$\rho = \sum_{\alpha=1}^{n} f_\alpha, \qquad \rho\,\mathbf{u} = \sum_{\alpha=1}^{n} \mathbf{e}_\alpha f_\alpha \tag{3}$$

A Chapman-Enskog expansion is applied to Eq. (2), by first making a Taylor series expansion of the first term. A scaling analysis is then applied to the zero-th and first moments of the resulting equation, showing that the LBM solution satisfies the incompressible NS equations within $\mathscr{O}(\Delta x^2)$ and $\mathscr{O}(\mathrm{Ma}^2)$ errors (see, e.g., Banari et al., 2014) provided the equilibrium DFs are selected as,

$$f_\alpha^{eq}(\rho,\mathbf{u}) = w_\alpha\left(\rho + \rho_0\left(3\frac{(\mathbf{u}\cdot\mathbf{e}_\alpha)}{c^2} + \frac{9}{2}\frac{(\mathbf{u}\cdot\mathbf{e}_\alpha)^2}{c^4} - \frac{3}{2}\frac{\mathbf{u}^2}{c^2}\right)\right) \tag{4}$$

where, ρ_0 and ρ represent the average fluid density and a small perturbation from that density, respectively, and w_α are lattice dependent directional weights with, $w_0 = 1/3$, $w_{1\ldots6} = 1/18$ and $w_{7\ldots18} = 1/36$. The relaxation time is then found as $\tau = 3\nu/c^2 + \Delta t/2$, a function of the fluid viscosity ν.

The collision step in Eq. (2) is a strictly local operation while the convective step propagates the particle distribution functions in their discretized velocity directions $\mathbf{e}_\alpha$ to neighboring lattice nodes. Unlike standard NS solvers used in CFD the LBM solution does not require a pressure correction step since pressure is directly found as $p = c_s^2\rho$. Both this locality of all numerical operations and the scaling of quantities so that finite differencing is not required makes the LBM very well suited to massively parallel computations on a GPGPU.

In their extension of the SRT-LBM, d'Humieres et al. (2002) showed that more accurate and stable results can be obtained, particularly for high Reynolds numbers Re, using the Multiple Relaxation Time (MRT) LBM. In this method, higher-order moments (i.e., hydrodynamic quantities and their fluxes) are incorporated into the solution, which have important physical significance (Lallemand and Lou, 2000) and will be useful to implement the LES in the LBM to more easily model turbulent flows at high Re numbers (see below). In the MRT, the collision operator in the right hand side of Eq. (2) is replaced by ($\beta = 0,...,18; \gamma,\delta = 0,...,15$; repeated indices in equations mean an implicit summation),

$$\Omega_\alpha = -M^{-1}_{\alpha\gamma} S_{\gamma\delta}(M_{\beta\delta} f_\beta - m^{eq}_\delta) \tag{5}$$

where $M_{\alpha\gamma}$ is the transformation matrix from DFs to moments, with $f_\alpha = M^{-1}_{\alpha\gamma} m_\gamma$ and $S_{\gamma\delta}$ is a diagonal collision matrix of relaxation parameters, weighing different properties of the fluid (see references). On this basis, equilibrium moments m^{eq}_γ are derived from the $f^{eq}_\alpha(\mathbf{x},t)$ as,

$$\begin{aligned}
m_0^{eq} &= \rho, \qquad m_3^{eq} = \rho_0 u_x, \qquad m_5^{eq} = \rho_0 u_y, \qquad m_7^{eq} = \rho_0 u_z \\
m_1^{eq} &= e^{eq} = \rho_0(u_x^2 + u_y^2 + u_z^2), \qquad m_9^{eq} = 3p_{xx}^{eq} = \rho_0(2u_x^2 - u_y^2 - u_z^2) \\
m_{11}^{eq} &= p_{zz}^{eq} = \rho_0(u_y^2 - u_z^2), \qquad m_{13}^{eq} = p_{xy}^{eq} = \rho_0(u_x u_y) \\
m_{14}^{eq} &= p_{yz}^{eq} = \rho_0(u_y u_z), \qquad m_{15}^{eq} = p_{xz}^{eq} = \rho_0(u_x u_z)
\end{aligned} \tag{6}$$

Equations for the perturbation LBM

Below, we summarize the expressions of the NS perturbation method applied to derive the hybrid LBM model formulation (Grilli, 2008; Harris and Grilli, 2012) and develop the corresponding LBM equations with the MRT. In the NS perturbation approach, both the flow velocity and pressure are expressed as the sum of inviscid and perturbation components,

$$u_i = u_i^I + u_i^P \qquad \text{with} \qquad \tilde{p} = \tilde{p}^I + \tilde{p}^P \tag{7}$$

where $\tilde{p} = p + \rho g z - \frac{2}{3}\rho k$ denotes the perturbation dynamic pressure, with k the turbulent kinetic energy. Superscripts I denote irrotational flow quantities, with $u_i^I = \nabla_i \phi^I$ satisfying Euler equations, and superscripts P represent perturbation flow quantities that are driven by the inviscid flow fields. Applying this decomposition to the NS equations and substituting Euler's equations, the perturbation NS equations read,

$$\frac{\partial u_i^P}{\partial x_i} = 0 \tag{8}$$

$$\frac{\partial u_i^P}{\partial t} + u_j^P \frac{\partial u_i^P}{\partial x_j} = -\frac{1}{\rho}\frac{\partial \tilde{p}^P}{\partial x_i} + (\nu + \nu_t)\frac{\partial^2 u_i^P}{\partial x_j \partial x_j} - \left(\frac{\partial u_i^I}{\partial x_j} u_j^P + u_j^I \frac{\partial u_i^P}{\partial x_j}\right) + 2\frac{\partial \nu_t}{\partial x_j} S_{ij} \tag{9}$$

where ν and ν_t are kinematic molecular and turbulent viscosity, respectively, with the latter being expressed through the Smagorinsky method as,

$$\nu_t = (C_S \Delta)^2 |\mathbf{S}|, \quad \text{with} \quad S_{ij} = S_{ij}^P + S_{ij}^I = \frac{1}{2}\left(\frac{\partial u_i^P}{\partial x_j} + \frac{\partial u_j^P}{\partial x_i} + \frac{\partial u_i^I}{\partial x_j} + \frac{\partial u_j^I}{\partial x_i}\right) \tag{10}$$

where C_S is the Smagorinsky constant, Δ a grid filtering length scale, and S_{ij} the rate of strain tensor, defined as the sum of components functions of the perturbation (S_{ij}^P) and inviscid (S_{ij}^I) velocity.

Janssen et al. (2010) developed a perturbation LBM-LES with MRT solving Eqs. (7) to (10), in which the "I-P" interactions terms were treated as volume forces through the B_α terms of Eq. (2). Here, instead, we solve these equations, assuming the perturbation LBM-LES DFs are also decomposed as, $f_\alpha = f_\alpha^I + f_\alpha^P$ and introduced in Eq. (2). Subtracting the LBM equation for the inviscid flow, we find,

$$f_\alpha^P(t+\Delta t, \mathbf{x} + \mathbf{e}_\alpha \Delta t)) - f_\alpha^P(t,\mathbf{x})) = -\frac{\Delta t}{\tau}\{f_\alpha^P(t,\mathbf{x}) - f_\alpha^{eq}(\rho^I + \rho^P, \mathbf{u}^I + \mathbf{u}^P) + f_\alpha^{eq,I}(\rho^I, \mathbf{u}^I)\} \tag{11}$$

where the $f_\alpha^{eq,I}(\rho^I, \mathbf{u}^I)$ are expressed with Eq. (4) based on inviscid fields and satisfy,

$$\sum_{\alpha=1}^{n} f_\alpha^{eq,I} = 0, \quad \sum_{\alpha=1}^{n} e_{\alpha i} f_\alpha^{eq,I} = \rho_0 u_i^I, \quad \sum_{\alpha=1}^{n} e_{\alpha i} e_{\alpha j} f_\alpha^{eq,I} = p^I \delta_{ij} + \rho_0 u_i^I u_j^I \tag{12}$$

The perturbation equilibrium DFs are then found as, $f_\alpha^{eq,P}(\rho^P, \mathbf{u}^P, \mathbf{u}^I) = f_\alpha^{eq}(\rho^I + \rho^P, \mathbf{u}^I + \mathbf{u}^P) - f_\alpha^{eq,I}(\rho^I, \mathbf{u}^I)$ with,

$$f_\alpha^{eq,P} = w_\alpha \left(\rho^P + \rho_0 \left(3\frac{\mathbf{u}^P \cdot \mathbf{e}_\alpha}{c_s^2} + \frac{9}{2}\frac{(\mathbf{e}_\alpha \cdot \mathbf{u}^P)^2 + 2(\mathbf{e}_\alpha \cdot \mathbf{u}^P)(\mathbf{e}_\alpha \cdot \mathbf{u}^I)}{c_s^4} - \frac{3}{2}\frac{(\mathbf{u}^P)^2}{c_s^2}\right)\right), \tag{13}$$

which satisfy,

$$\sum_{\alpha=1}^{n} f_\alpha^{eq,P} = \rho^P, \quad \sum_{\alpha=1}^{n} e_{\alpha i} f_\alpha^{eq,P} = \rho_0 u_i^P,$$

$$\sum_{\alpha=1}^{n} e_{\alpha i} e_{\alpha j} f_\alpha^{eq,P} = p^P \delta_{ij} + \rho_0 u_i^I u_j^P + \rho_0 u_i^P u_j^I + \rho_0 u_i^P u_j^P \tag{14}$$

A rigorous Chapman-Enskog expansion would show that the perturbation NS Eqs. (7) to (10) are recovered when using these DFs. Note the interaction terms between the I and P fields in Eqs. (13) and (14), expressing the inviscid flow forcing on the perturbation fields.

Extending this formulation to the MRT, assuming a collision operator expressed by Eq. (5), we find the equilibrium moments,

$$\begin{aligned}
m_1^{eq} = e^{eq} &= \rho_0((u_x^P)^2 + (u_y^P)^2 + (u_z^P)^2 + 2u_x^P u_x^I + 2u_y^P u_y^I + 2u_z^P u_z^I) \\
m_9^{eq} = 3p_{xx}^{eq} &= \rho_0(2(u_x^P)^2 - (u_y^P)^2 - (u_z^P)^2 + 4u_x^P u_x^I - 2u_y^P u_y^I - 2u_z^P u_z^I) \\
m_{11}^{eq} = p_{zz}^{eq} &= \rho_0((u_y^P)^2 - (u_z^P)^2 + 2u_y^P u_y^I - 2u_z^P u_z^I) \\
m_{13}^{eq} = p_{xy}^{eq} &= \rho_0(u_x^P u_y^P + u_x^P u_y^I + u_y^P u_x^I) \\
m_{14}^{eq} = p_{yz}^{eq} &= \rho_0(u_y^P u_z^P + u_y^P u_z^I + u_z^P u_y^I) \\
m_{15}^{eq} = p_{xz}^{eq} &= \rho_0(u_x^P u_z^P + u_x^P u_z^I + u_z^P u_x^I)
\end{aligned} \tag{15}$$

Moments that are not listed above are unchanged from the standard MRT formulation.

LES turbulence modeling with a LBM

Implementing a LES into the LBM requires evaluating the rate of strain tensor S_{ij}. To do so, Krafczyk et al. (2003) showed that the 2nd-order moments of the DFs can be expressed as,

$$P_{ij} = \sum_{\alpha=1}^{n} e_{\alpha i} e_{\alpha j} f_\alpha = c_s^2 \rho \delta_{ij} + \rho_0 u_i u_j - \frac{2c_s^2 \rho_0}{s_2} S_{ij} \tag{16}$$

where s_2 is a relaxation rate for these moments, and showed that they are related to 2nd-order moments in the MRT, $3p_{xx}$, p_{zz}, p_{xy}, p_{yz}, and p_{xz}. The 1st and 2nd terms in Eq. (16)'s RHS are functions of flow quantities obtained through other moments of the DFs. Based on Eq. (16), the rate of strain tensor can thus be expressed as,

$$S_{ij} = \frac{s_2}{2c_s^2 \rho_0}\{c_s^2 \rho \delta_{ij} + \rho_0 u_i u_j - P_{ij}\} = \frac{s_2}{2c_s^2 \rho_0} Q_{ij} \tag{17}$$

where Q_{ij} are the terms in $\{\}$. Krafczyk et al. (2003) assumed that the Q_{ij}'s are functions of the non-equilibrium part of the DFs, $f_\alpha^{neq} = f_\alpha - f_\alpha^{eq}$ and provided their expressions as a function of the 2nd-order MRT moments. Applying Eq. (10), they then calculated the LES turbulent viscosity as,

$$\nu_t = (C_S \Delta)^2 |\mathbf{S}| = \frac{s_2}{2c_s^2 \rho_0}(C_s \Delta)^2 |\mathbf{Q}|, \quad \text{with} \quad |\mathbf{Q}| = \sqrt{Q_{ij} Q_{ij}} \tag{18}$$

with the relaxation rate of the 2nd-order moments defined as,

$$s_2 = \frac{1}{\tau_0 + \tau_t} \quad \text{with} \quad \tau_t = \frac{1}{2}\left(\sqrt{\tau_0^2 + 18(C_s\Delta)^2 |\mathbf{Q}|} - \tau_0\right) \tag{19}$$

where τ_0 is the relaxation time based on the molecular viscosity.

When applying the LES to the perturbation LBM, the moments P_{ij}^P are given by the last Eq. (14), yielding an expression for the perturbation rate of strain tensor that features nonlinear interaction terms between the I and P fields,

$$S_{ij}^P = \frac{s_2}{2c_s^2 \rho_0}\left(c_s^2 \rho^P \delta_{ij} + \rho_0 u_i^P u_j^P + \rho_0 u_i^I u_j^P + \rho_0 u_i^P u_j^I - P_{ij}^P\right) = \frac{s_2}{2c_s^2 \rho_0} Q_{ij}^P$$

(20)

The rate of strain tensor for the total flow is finally given by,

$$S_{ij} = \frac{s_2}{2c_s^2\rho_0} Q_{ij}^P + S_{ij}^I \tag{21}$$

Therefore the $|\mathbf{Q}|$ term to use in LES Eqs. (18) and (19), in combination with the MRT LBM Eqs. (11) to (15), is found as follows,

$$|\mathbf{Q}| = \sqrt{R_{ij}R_{ij}} \qquad \text{with} \qquad R_{ij} = Q_{ij}^P + \frac{2c_s^2\rho_0}{s_2} S_{ij}^I \tag{22}$$

where the Q_{ij}^P terms are computed with Eq. (20).

LBM turbulent wall model

Typical naval hydrodynamics flows are fully turbulent, with $\mathrm{Re} > 10^6$. Thus, the turbulent boundary layers (BL) near solid boundaries (e.g., ship hull) must be properly modeled in the LBM. Since resolving the BL in the LBM grid would be computationally prohibitive (even with grid refinement through nesting such as done in ELBE), besides the LES of the flow, this requires implementing a turbulent a wall model.

Below, we describe the extension to the perturbation LBM-LES of the method proposed by Malaspinas and Sagaut (2014), based on a macroscopic representation of the flow within the BL (i.e., on the LBM lattice). A thin layer approximation is introduced, implying that the mean free flow is locally nearly parallel to the solid boundary (i.e., wall) and statistically stationary; it is also assumed that there is no horizontal pressure gradient. In such conditions, the mean velocity profile can be found as a function of the distance to the wall y from the semi-empirical equation proposed by Musker (1979), on the basis of experimentally validated logarithmic "laws of the wall" for the fully turbulent upper BL, the viscous lower BL, and a transition layer,

$$\begin{aligned} \tilde{u}(y^+) &= u_\tau \Bigg(\Bigg(5.424 \operatorname{atan}\left(\frac{2.0y^+ - 8.15}{16.7} \right) \\ &+ \log_{10}\left(\frac{(y^+ + 10.6)^{9.6}}{(y^{+2} - 8.15y^+ + 86.0)^2} \right) - 3.52 \Bigg) \end{aligned} \tag{23}$$

where the friction velocity u_τ and non-dimensional distance y^+ are defined as,

$$u_\tau = \sqrt{\tau_w/\rho} \qquad \text{and} \qquad y^+ = y\frac{u_\tau}{\nu} \tag{24}$$

where y is aligned with the wall normal. Malaspinas and Sagaut (2014) also express the turbulent eddy viscosity as

$$\nu_t = \kappa(\Delta x) y \left(1 - e^{\frac{-y^+}{26.0}} \right)^2 \left| \frac{\partial \tilde{u}}{\partial y} \right| \tag{25}$$

where κ is a constant chosen to be 0.384 based on experimental data and $\Delta x = 1$ is mesh size.

The "law of the wall" Eqs. (23) to (25) will be used to express the boundary condition near a solid boundary in the LBM, where unknown DF's are reconstructed on the lattice nodes based on the macroscopic flow quantities. Let us define $\mathbf{x}_1$, $\mathbf{x}_2$, and $\hat{\mathbf{n}}$ as the position of the first and second off wall lattice nodes and the outward normal unit vector at the wall, respectively (Fig. 1). As is standard in most LBM wall boundary models, DF's that satisfy $\mathbf{e}_\alpha \cdot \hat{\mathbf{n}} < 0$ (dashed populations seen in Fig. 1b) are assumed to be unknown after the propagation step and must be reconstructed. This is done using the macroscopic flow quantities, ρ_1, $\mathbf{u}_1$ and $\partial \mathbf{u}_1/\partial y$, calculated using the "law of the wall".

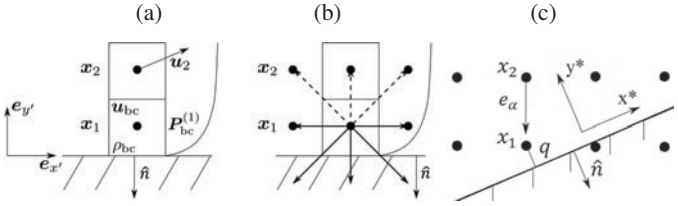

Fig. 1: Sketch of LBM flow reconstruction near a solid boundary (assumed 2D for simplicity): (a) known or computed variables; (b) known (——) and missing (- - - -) DF populations; (c) variables in geometric calculations. Lattice points are marked by (•). [(a) and (b) from Malaspinas and Sagaut (2014)]

The DFs near the wall are thus constructed as,

$$f_\alpha(\mathbf{x}_1, t) = f_\alpha^{eq}(\rho_1, \mathbf{u}_1) + f_\alpha^{neq}\left(\frac{\partial \tilde{\mathbf{u}}_1}{\partial y} \right) \tag{26}$$

where f_α^{eq} are specified through Equations (2) and (13) for the standard LBM or the perturbation LBM methods, respectively. The f_α^{neq} DFs are constructed as follows (Malaspinas and Saugat 2014),

$$f_\alpha^{neq}\left(\frac{\partial \tilde{\mathbf{u}}_1}{\partial y} \right) = -\frac{w_\alpha \rho_0}{c_s^2 \lambda_\nu} \sum_{i=1}^{3} \sum_{j=1}^{3} \{ e_{\alpha i} e_{\alpha j} - c_s^2 I_{ij} \} S_{ij} \tag{27}$$

where λ_ν is the laminar relaxation time and I_{ij} is the identity matrix.

To evaluate $\mathbf{u}_1$, which depends on the wall shear stress τ_w, for each near-wall lattice point, one numerically solves the implicit equation, $u_2^* = \tilde{u}(y_2, \tau_w)$ where u_2^* is calculated as the magnitude of the velocity projected in the tangential direction to the wall $u_2^* = |\mathbf{u}_2 \cdot \hat{\mathbf{t}}|$ ($\hat{\mathbf{t}}$ being the unit local tangential vector). A Newton iteration scheme is used to find $\tilde{u}(y_2', \tau_w)$, given by Musker's Eqs. (23) and (24), which iterates over the τ_w value until convergence is achieved.

Next $\tilde{\mathbf{u}}_1$ and ν_1 are solved for and $\mathbf{u}_1$ is found by projecting $\tilde{\mathbf{u}}_1$ along the unit local tangential vector, $\mathbf{u}_1 = (\tilde{\mathbf{u}}_1 \cdot \hat{\mathbf{t}})\hat{\mathbf{t}}$. The BL turbulent viscosity, ν_1, is used to calculate the relaxation rate of the 2nd-order moments as $s_2 = 1/(\tau_0 + \nu_1)$, replacing the LES Eq. (19). Finally, ρ_1 is calculated by reconstructing the flow density based on known DFs only,

$$\rho_1 = (\rho_\alpha + \rho_\beta), \qquad \text{with} \qquad \rho_\alpha = \sum_\alpha f_\alpha \qquad \text{and} \qquad \rho_\beta = \sum_\beta f_{\beta^*} \tag{28}$$

Where lattice links along directions α do not intersect the wall, lattice links along directions β intersect the wall, and directions β^* are the opposite directions to β. Equation (26) may now be applied to the unknown DFs.

When using this method for general boundary geometries, a shift in reference frame is needed, such that the x-axis points towards the local streamwise direction and locations $\mathbf{x}_1$ and $\mathbf{x}_2$ align with the wall normal. Thus, a wall normal projection is applied to determine location $\mathbf{x}_2$,

$$y_\alpha^* = \frac{\mathbf{e}_\alpha \cdot -\hat{\mathbf{n}}}{|\mathbf{e}_\alpha|} \tag{29}$$

The direction α with the largest y_α^* is chosen to find $\mathbf{x}_2$ as, $\mathbf{x}_2 = \mathbf{x}_1 + \mathbf{e}_\alpha \Delta t$. Although $\mathbf{x}_1$ and $\mathbf{x}_2$ will not perfectly align with the wall normal when the lattice and wall are not coincident, such as in Fig. 1c, a small loss of accuracy due to geometry is acceptable. The distance, q, between the first node $\mathbf{x}_1$ and the nearest location on the solid boundary (see Fig. 1c) is used in the calculation of y^+ (Eq. (24)). The wall normal distances to $\mathbf{x}_1$ and $\mathbf{x}_2$ are then defined as q and $|(\mathbf{e}_\alpha \cdot \hat{\mathbf{n}})\Delta t| + q$, respectively. At

all $\mathbf{x}_1$ locations, the q values are computed using a Newton scheme and a polynomial fitted to describe the local wall boundary geometry (such as the NACA0012 profile modeled below); both directions $\hat{\mathbf{n}}$ and $\hat{\mathbf{t}}$ are also computed using this polynomial at the location coinciding with the minimized distance q.

In general, as the wall normal distance y decreases, f_α^{eq} will decrease and f_α^{neq} will increase, potentially violating the scaling assumptions made in the Chapman-Enskog expansion to recover the Navier-Stokes equations. Therefore, a limitation must be imposed on the wall model as q decreases. It has been found that, in order to correctly capture the velocity profile in the turbulent channel simulations described below, distance q must be greater than $0.2\Delta x$. Additionally, in regions where the y^+ value is less than 5, the viscous sublayer of the turbulent profile is reached and a standard bounce back condition is suitable. This is particularly important in regions of flow separation or near stagnation points.

When applying the turbulent wall model to the perturbation LBM, we reconstruct the total flow, $\mathbf{u}_2$, from $\mathbf{u}_2 = \mathbf{u}_2^I + \mathbf{u}_2^P$, and solve the macroscopic (Musker) equation to find $\mathbf{u}_1 = \mathbf{u}_1^I + \mathbf{u}_1^P$. The equilibrium DFs in Eq. (26) are now those of Eq. (13). Furthermore, in Eq. (27) we now use S_{ij}^P instead of S_{ij}, so that only the perturbation component is applied back to the DF's. Finally if, the wall model is not applied, a standard "bounce forward" scheme is used, satisfying a no-slip condition for the total velocity, $\mathbf{u}^P = -\mathbf{u}^I$,

$$f_{\alpha'}(\mathbf{x}_1,t) = f_\alpha(\mathbf{x}_1,t) - 2\rho_0 w_\alpha \frac{\mathbf{e}_\alpha \cdot -\mathbf{u}^I}{c^2} \tag{30}$$

where direction α' is opposite to direction α.

LBM and Hybrid LBM force evaluation

The total force acting on a solid body is computed in the perturbation LBM as a linear combination of the inviscid and perturbation forces, $\mathbf{F} = \mathbf{F}^I + \mathbf{F}^P$, where the inviscid contribution is evaluated through an integration over the body boundary Γ_B of the known pressure p^I. The perturbation force may be calculated in a manner that is consistent with typical LBM simulations. In the following results, the stress integration method has been used to evaluate forces

$$\mathbf{F} = \iint_S \{p\hat{\mathbf{n}} + \tau_\mathbf{w}\}\, dS \tag{31}$$

where $\hat{\mathbf{n}}$ is the unit normal vector on the surface. Discretizing the above equation yields

$$\mathbf{F} = \sum \{p\hat{\mathbf{n}} + \tau_\mathbf{w}\}\Delta S \tag{32}$$

where, ΔS represents a discretized surface area, a function of $(\Delta x)^2$, and $p = c_s^2\rho$ a function of the first-order moment of the DFs. A common method for calculating $\tau_\mathbf{w}$ in LBM is to use the non-equilibrium component of the second-order moment using Eq. (17) where

$$\tau_i = \mu \sum_{j=1}^{3} S_{ij} \tag{33}$$

This direct evaluation, using the DFs and their moments, eliminates a loss of accuracy that would otherwise occur from the cancellation of two close numbers in f_α during the calculation of $\mathbf{u}$ and subsequent $\partial\mathbf{u}/\partial\mathbf{x}$ (Mei et al., 2002). However, since a Cartesian grid is used, the stress vectors acting on the surface of the body have to be extrapolated based on the information at the nearest fluid lattice nodes, leading to a loss of accuracy, particularly at high y^+ values. Here, we eliminate this error by applying $\tau_\mathbf{w}$ calculated exactly at the wall boundary using the Musker profile, in Eq. (32). At boundary locations where the turbulent wall model is not applied, Eq. (33) is used in Eq. (32).

APPLICATIONS

Simulation of turbulent flow over a flat plate

Here, we validate the turbulent wall model in the context of the perturbation LBM by simulating a turbulent flow over a flat plate; results are compared to those of the standard LBM. A key difference between the results presented here and those presented previously (O'Reilly et. al (2016) and Malaspinas and Sagaut's (2014)) is that a generalized force evaluation method based on Eq. (32) is used. Similar to Malaspinas and Sagaut's (2014) test case, we use a parallelepipedic domain of dimensions, $L = 2\pi M$, $H = 2M$, and $W = 2\pi M$ (M denoting the half channel width), with flat plates specified on the lower/upper boundaries at $y = 0$ and H, on which the turbulent wall model is applied, and periodic boundary conditions in the 2 horizontal directions at $x = 0$ and L (streamwise) and $z = 0$ and W (cross stream). In this application, the flow is forced by way of a body force (term B_α in LBM Eq. (2); see, Cabrit, 2009), $F = \{u_\tau^2 + u_m(u_m - u_x)\}/M$, in which u_x is the instantaneous space-averaged downstream velocity component. The inviscid velocity field specified in the perturbation LBM is uniform over the channel, $\mathbf{u}^I = U$, where U is calculated by applying the law of the wall Eq. (23) at the center of the channel, i.e., $\tilde{u}(y^+)$ for $y = H/2$. The Smagorinsky constant used in the LES is $C_S = 0.16$ in all simulations, which is in the middle of the range of recommended values. Each simulation is run until both a fully turbulent flow is observed and a quasi-steady mean flow is achieved. We tested flows for 3 values of the Reynolds number, $\mathrm{Re}_\tau = Mu_\tau/\nu = 950$, 2,000, and 20,000 based on the friction velocity u_τ, or $\mathrm{Re}_m = 2Mu_m/\nu = 37{,}042$, 86,773, and 1.21×10^6 based on the average bulk velocity u_m in the x direction, obtained from Dean's (1976) correlation. Each case was simulated in 4 LBM discretizations, for which $\Delta x = \Delta y = \Delta z = M/N$, with $N = 10$, 20, 30, and 40. The full channel width is thus discretized with $2N$ LBM points in the y direction.

Figure 2a shows the velocity profiles computed for $\mathrm{Re}_\tau = 2{,}000$ with the perturbation LBM-LES. In the interest of saving space, results from only one Re_τ are shown and a more complete set of velocity profile results may be found in O'Reilly et al. (2016). Almost identical results were obtained using the standard LBM-LES, which further confirms the relevance and accuracy of the decomposition method. In all cases, the perturbation LBM-LES results agree well with Musker's (1979) profile for the smaller y^+ values, which is expected. At higher y^+ values, however, velocities are slightly smaller in the LBM than in the experimental profile, which is likely the result of having 2 plates in the model, with a finite separation distance H, rather than a free flow past a single plate, which is the case of Musker (1979).

Using the law of the wall to specify the boundary condition just above the solid boundary, we see that the LBM-LES is able to accurately capture the velocity profile in the intermediate and turbulent BLs, without need for a fine discretization and in particular for resolving the viscous BL. For the largest Re, the method is pushed to its limits, with the resolution being such that $y_1^+ = 333$, 500, and 1000 at the first LBM point ($\mathbf{x}_1$ in Fig. 1), for the different N values, which is quite large; the latter is a very under-resolved test, but one that demonstrates the overall robustness of the method.

The computed bulk friction coefficient presented in earlier work (O'Reilly et al (2016) and Malaspinas and Sagaut (2014)) uses Dean's (1976) correlation $C_f = 2u_\tau^2/u_m^2$, which is based on experiments and applicable only to this test case. Fig. 2b shows a validation of our force evaluation method, applicable to a generalized geometry, which uses Eq. (32) to evaluate the drag force. Here, we calculate the friction coefficient as, $C_f = F_d/(\frac{1}{2}\rho u_m^2 A)$, with A being the wetted area of the top and bottom walls. In the figure, the calculated results are compared to the

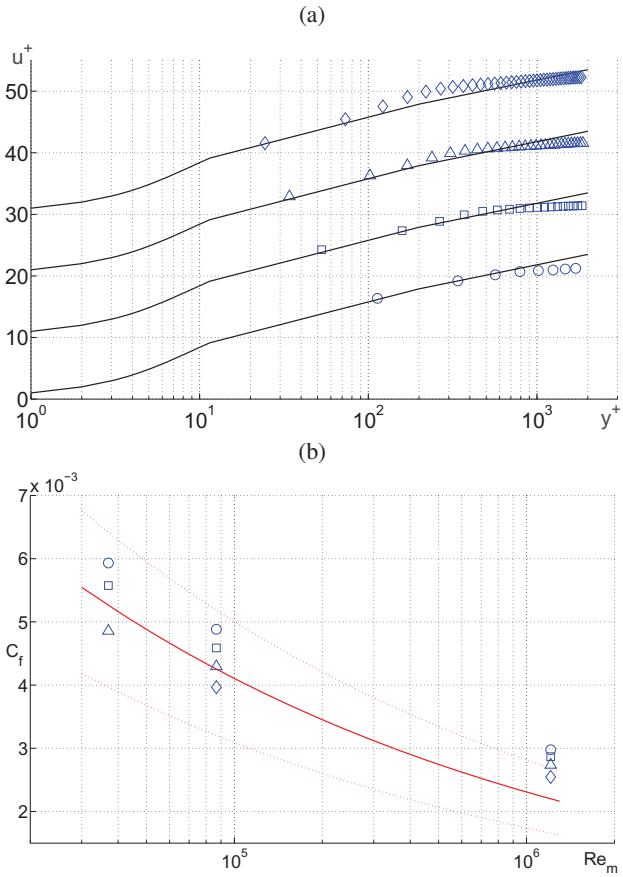

Fig. 2: Simulation of turbulent flow past a flat plate with the perturbation LBM. (a) Mean velocity u^+ as a function of distance y^+ above the plate, at Re_m =86,773. Numerical results (symbols) are plotted for a half channel of resolution $N = (\circ)$ 10, $(\square)$ 20, $(\triangle)$ 30, and $N = 40$ $(\diamond)$, compared to Musker's (1979) velocity profile (——). For visualization purposes, results for $N = 20$, 30, and 40 are shifted by $\Delta u^+ = 10$, 20, and 30, respectively. (b) Friction coefficient C_f computed, compared to Dean's (1976) correlation for turbulent channels (——) and the upper and lower bounds of his measurements (- - -).

measured Dean's correlation, with the upper and lower bounds of measurements being marked to indicate the experimental variance, within which any numerical result should be deemed acceptable. Drag coefficients for $\mathrm{Re}_\tau = 950$ and 2,000 are within the experimental variance at all resolutions; for $\mathrm{Re}_\tau = 20,000$, convergence also occurs with resolution, but only the highest resolution result falls within the experimental variance. Finally, there is again negligible differences between C_f values calculated with the standard LBM or the perturbation LBM models.

Simulation of turbulent flow around a submerged hydrofoil

Here, we test the accuracy and efficiency of the perturbation LBM, as compared to the standard LBM, with LES and a wall model, and particularly the accuracy of the force computations by Eq. (32). This is done by simulating turbulent flows around a NACA0012 foil (Fig. 3) as a function of its angle of attack θ, for a Reynolds number $\mathrm{Re} = UC/\nu = 1\times10^6$ (with U the free flow velocity, C the foil chord, and $\nu = 10^{-6}$ the water kinematic viscosity). We solve this as a 3D problem by placing the foil in a channel of length L, height H, and width W (Grid 0, Table 1). We compute both the lift and drag forces on the foil, $F_L = (1/2)\rho U^2 C_L WC$ and $F_D = (1/2)\rho U^2 C_D WC$, respectively, and parameterize them as usual as a function of a lift and drag coefficient, C_L and C_D, respectively. While previous results (O'Reilly et al., 2016) have shown that the force computation method with Eq. (32) can predict an accurate lift force for a similar test setup without a wall model, the drag force predicted in earlier work was not realistic. Predicting lift for this foil, which is dominated by differences in pressure distribution, is in fact significantly easier than predicting drag, which is dominated by both shear and pressure forces and can be more than an order of magnitude smaller than lift. Results below will show that the combination of an improved sub-grid turbulence modeling with more accurate shear estimates provided by the turbulent wall model, yields more accurate drag estimates in the present simulations.

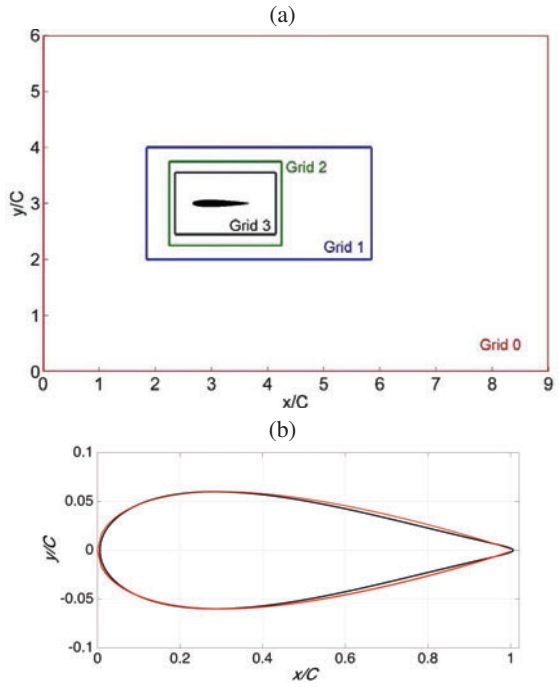

Fig. 3: (a) Nested LBM grid boundaries (Table 1). (b) cross-sections of a: (——) NACA0012 foil; and (——) Karman-Trefftz foil used to compute the potential flow solution.

Grid Number	L/C	W/C	H/C	$\Delta x/C$	N
Grid 0	9.0	6.0	0.2	0.0226	1,068,000
Grid 1	4.0	2.0	0.18	0.0113	1,153,440
Grid 2	2.0	1.5	0.16	0.0056	2,862,240
Grid 3	1.8	1.1	0.14	0.0028	13,045,760

Table 1: Grid parameters of the domain used in the tests of the regular and hybrid LBM-LES models, for the submerged hydrofoil test case (Figs. 3 and 4). Grid length is L, width W, height H, and hydrofoil chord length C. Total number of LBM points is $N = 18,129,440$.

In all cases we use nested LBM grids, increasingly resolved towards the foil: 4 for the standard LBM and 3 for the perturbation LBM (Table 1 and Fig. 3a); this domain discretization is near the largest possible, considering the 5GB of available memory in our current GPGPU. LBM results indicate that convergence in lift and drag forces was not achieved, which would require a larger domain. At zero angle of attack the maximum y^+ value found was approximately 50 and all simulations were run using Ma= 0.01. Boundary conditions were specified as follows, for the standard or perturbation LBMs, respectively: (i) periodic conditions on sidewall boundaries ($z = 0$ and W); (ii) a specified velocity $\mathbf{u} = U$ on the inlet/outlet ($x = 0$ and $x = L$) and upper/bottom boundaries ($y = 0$ and H); (iii) and a turbulent wall model on the foil boundary Γ. In the LBM, periodicity is achieved by specifying periodic DFs, and velocity is prescribed on a boundary by specifying the DFs as $f_\alpha = f_\alpha^{eq}(\rho, \mathbf{u})$.

The inviscid fields ($\mathbf{u}^I$, p^I) are analytically calculated at each LBM node based on a conformal mapping solution for a Karman-Trefftz foil that is very similar in shape to the NACA0012 foil (Fig. 3b). In future more complex cases this solution will be computed with an inviscid BEM model (see Mivehchi et al. in this conference). Using the discretizations of Tables 1 and Fig. 3a, the LBM and perturbation LBM methods need approximately 13 hours and 7 hours, respectively, on an NVIDIA® Tesla® K20 GPGPU to simulate approximately 3 seconds of steady state, at 0 degrees angle of attack.

Fig. 4a shows the foil lift coefficient C_L computed as a function of θ with various methods, as compared to laboratory experiments in a wind tunnel by Sheldah and Kilmas (1981) and Gregory and O'Reilly (1973). Note that the discrepancies observed between different measurements made for the same angle reflect both experimental uncertainties and Reynolds number effects. A good agreement is observed for the potential flow solution at low angles of attack $\theta \leq 8$ deg.; this is expected in this high Re number regime. However at larger angles of attack, flow separation starts occurring with increased viscous/turbulent effects and the inviscid solution overpredicts lift and misses stall. The LBM solution with the wall model predicts C_L well from 0 deg. to 8 deg., but then slightly under predicts lift at 12 deg. At higher angles of attack, the turbulent wall model delays flow separation and stall along the low pressure side of the foil and increases lift relative to the LBM solution without a wall model (see O'Reilly et al. 2016). Consistent with earlier results by O'Reilly et al. (2016), the perturbation LBM solution is close to experimental results, even when applied to the reduced size domain. At 12 deg, the hybrid LBM solution overpredicts lift because of reduced flow separation on the low pressure side of the foil resulting from the inviscid forcing. However an unsteady lift force was observed, indicating vortex shedding and the onset of stall.

Fig. 4b similarly shows the foil drag coefficient C_D computed as a function of θ with various methods, as compared to laboratory experiments. The potential flow solution (not shown) predicts zero drag because of d'Alembert paradox. The LBM and perturbation LBM results predict a drag coefficient at 0 deg incidence, up to twice that measured in the reference solutions (Sheldah and Kilmas, 1981 and Gregory and O'Reilly, 1973, in which the boundary layer development was allowed to transition naturally from laminar to turbulent). However, the laminar to turbulent transition is not modeled in our results and the boundary layer is assumed to be fully turbulent downstream of 10% of the chord. As expected, our results better agree with drag measurements where turbulence was tripped at the same location on the foil (Gregory and O'Reilly, 1973). Furthermore, Gregory and O'Reilly (1973) show that as the Reynolds number decreases, C_D increases and our results follow this trend. For the LBM solution without inviscid forcing, as the angle of attack increases, the pressure drag also increases at a rate that is too large as compared to experiments; our results show that the addition of a wall model reduces this error. Additional errors in drag are likely because the outer domain boundaries may still be too close to the foil. Furthermore the wall model could be improved by using a boundary layer equation that considers an adverse pressure gradient when flow separation occurs. Consistent with previous results (O'Reilly et al 2016), the perturbation LBM results for C_D are closer to the experimental measurements than the LBM results, particularly as the angle of attack increases. The C_D for the LBM and hybrid LBM solutions at 12 deg (not shown) are 0.245 and 0.189, respectively.

These results for both C_L and C_D confirm the advantages of the hybrid LBM method, with the inviscid flow forcing the viscous solution and allowing for both a more accurate computation of the total flow and a reduced computational time.

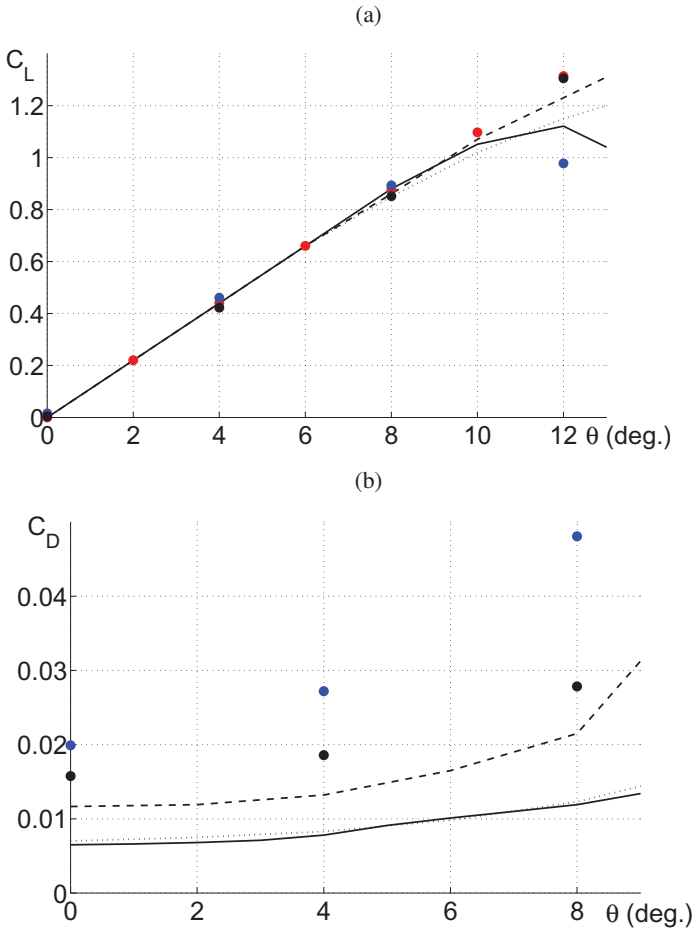

Fig. 4: (a) Lift and (b) drag coefficient of a NACA0012 foil, as a function of its angle of attack, in wind tunnel experiments (lines) and computations for Re = $UC/\nu = 1 \times 10^6$ (U is flow velocity, C is chord length, and ν the fluid kinematic velocity) with a: (•) potential flow method; (•) LBM; (•) perturbation LBM. Experimental results are from: Sheldah and Kilmas (1981) for Re = 1×10^6 (——); Gregory and O'Reilly (1973) at Re=0.88×10^6 for natural boundary layer transition tests (...) and Re=1.44×10^6 for tripped turbulent boundary layer tests (- - -).

CONCLUSIONS

We presented the formulation and simulation results for a new hybrid model combining potential flow and NS-LBM-LES solvers, that is aimed at solving naval hydrodynamics problems. In this paper, only simple applications were presented for a submerged foil and a turbulent channel, that demonstrated both the relevance and accuracy of the hybrid approach. In particular, we showed a close agreement between results of the standard and perturbation LBM-LES models, and between both of these and experimental data. However, for the perturbation approach, this could be achieved more efficiently in a reduced size domain.

While the inviscid rate of strain tensor was zero by construction in the turbulent channel simulations, it was present and provided a significant contribution to shear near the solid boundary in the turbulent hydrofoil simulations. Follow-up work, that will be presented at the conference, will include a more comprehensive validation of the hydrofoil case by increasing the grid resolution near to the foil and by further reducing the domain size using the hybrid method. Furthermore the limits of the hybrid LBM-LES formulation will be tested through a hydrofoil simulation

using a potential flow solution with zero circulation, thus zero lift. In this case the perturbation solution is a more substantial component of the total flow and must provide the entire lift force. Additionally, in future work, we will model more complex geometries for both submerged and surface piercing bodies.

The main advantage of the perturbation LBM is its ability to use a smaller domain to solve the NS equations relative to standard solvers, hence allowing for both higher resolution and efficiency. Although illustrated for the submerged hydrofoil case, the hybrid approach was not strictly necessary owing to the simple flow and geometry. However, once we consider surface piercing advancing bodies, which will cause the generation of surface gravity waves, and whose far-field can be well represented by an inviscid model, the benefits of the hybrid modeling approach will become much more significant; this was illustrated in preliminary work using ELBE, reported in O'Reilly et al. (2015).

Such cases will also be the object of future work, with the ultimate goal being to model seakeeping problems for multiple degree-of-freedom floating bodies advancing in strongly nonlinear irregular wave fields. One main challenge to address in such problems will be to extend the perturbation LBM method to include fully non-linear free surface boundary conditions, in which "I-P" interaction terms will appear.

ACKNOWLEDGEMENTS

C. O'Reilly, S.T. Grilli, A. Mivehchi and J. Dahl gratefully acknowledge support for this work from grants N000141310687 and N000141612970 of the Office of Naval Research (PM Kelly Cooper).

REFERENCES

Alessandrini, B. (2007). *Thèse d'Habilitation en Vue de Diriger les Recherches*. Ecole Centrale de Nantes, Nantes.

Banari A., Janssen C.F., and Grilli S.T. (2014). An efficient lattice Boltzmann multiphase model for 3D flows with large density ratios at high Reynolds numbers. *Comp. and Math. with Applications*, **68**(12), 1819-1843.

Cabrit, O. (2009) Direct simulations for wall modeling of multicomponent reacting compressible turbulent flows. *Physics of Fluids*, **21**, 055108.

Dean, R. B., (1976) A single formula for the complete velocity profile in a turbulent boundary layer. *J. Fluids Eng.*, **98**(4), 723-726.

Gregory, N., O'Reilly, C. L., (1973) Low-Speed Aerodynamic Characteristics of NACA 0012 Aerofoil Section, including the Effects of Upper-Surface Roughness Simulating Hoar Frost. *Ministry of Defence Aeronautical Research Council Reports and Memoranda.*, No. 3726.

Grilli, S.T. (2008) On the Development and Application of Hybrid Numerical Models in Nonlinear Free Surface Hydrodynamics. Keynote lecture in *Proc. 8th Intl. Conf. on Hydrodynamics* (Nantes, France, 9/08) (P. Ferrant and X.B. Chen, eds.), pps. 21-50.

Grilli, S.T., Dias, F., Guyenne, P., Fochesato, C. and F. Enet (2010) Progress In Fully Nonlinear Potential Flow Modeling Of 3D Extreme Ocean Waves. Chapter 3 in *Advances in Numerical Simulation of Nonlinear Water Waves* (ISBN: 978-981-283-649-6, edited by Q.W. Ma) (Vol. 11 in Series in Advances in Coastal and Ocean Engineering). World Scientific Publishing Co. Pte. Ltd., pps. 75- 128.

Guo Z., Zheng C., and Shi B. (2002). Discrete lattice effects on the forcing term in the lattice Boltzmann method. *Phys. Rev.*, **E65**(4).

Harris, J.C. and S.T. Grilli (2012). A perturbation approach to large-eddy simulation of wave-induced bottom boundary layer flows. *Intl. J. Numer. Meth. Fluids*, **68**, 1,574-1,604.

Harris J.C. and Grilli, S.T. (2014). Large eddy simulation of sediment transport over rippled beds. *Nonlin. Process. Geophys.*, **21**, 1,169-1,184.

d'Humieres D., Ginzburg I., Krafczyk M., Lallemand P., and Luo L.-S. (2002) Multiple Relaxation-Time Lattice Boltzmann models in three-dimensions. *Phil. Trans. Royal Soc. London*, **A360**, 437-451.

Janssen C.F., S.T. Grilli and M. Krafczyk (2010) Modeling of Wave Breaking and Wave-Structure Interactions by Coupling of Fully Nonlinear Potential Flow and Lattice-Boltzmann Models. In *Proc. 20th Offshore and Polar Engng. Conf.* (ISOPE10, Beijing, China, June 20-25, 2010), pps. 686-693. Intl. Society of Offshore and Polar Engng.

Janssen, C.F. (2010) *Kinetic approaches for the simulation of non-linear free surface flow problems in civil and environmental engng.*. PhD thesis, Technical Univ. Braunschweig.

Janssen, C.F., S.T. Grilli and M. Krafczyk (2013) On enhanced nonlinear free surface flow simulations with a hybrid LBM-VOF approach. *Comp. and Math. with Applications*, **65**(2), 211-229.

Janssen, C.F., D. Mierke, M Überrück, S. Gralher, and T. Rung (2015) Validation of the GPU-accelerated CFD solver ELBE for free surface flow problems in civil and environmental engineering. *Computation*, **3**(3),354-385.

Janssen, C.F., Rung, T., Grilli S.T., O'Reilly C.M., (2017) An enhanced LBM-based perturbation method (in preparation).

Krafczyk M., Tölke J., Rank E., and Schulz M. (2001) Two-dimensional simulation of fluid-structure interaction using Lattice Boltzmann methods. *Comp. and Struct.*, **22**, 2,031-2,037.

Krafczyk M., Tölke J., and Luo L.-S. (2003) Large eddy simulations with a multiple-relaxation-time LBE model. *Intl. J. Modern Phys.*, **17**, 33-39.

Lallemand, P. and Luo, L.S. (2000) Theory of the Lattice Boltzmann Method: Dispersion, dissipation, isotropy, Galilean invariance, and stability. *Phys. Review*, **E61**, 6,546-6,562.

Malaspinas, O., Sagaut, P., (2014) Wall model for large-eddy simulation based on the lattice Boltzmann method. *J. Comp. Phys.*, **257**, 25-40.

Merkle, D., Janssen, C.F., (2016) Efficient calculation of sub-grid distances for higher-order boundary conditions in LBM (to be submitted).

Musker, A. (1979) Explicit expression for the smooth wall velocity distribution in a turbulent boundary layer. *AIAA J.*, **17**(6), 655-657.

O'Reilly, C., Grilli, S.T., Dahl, J.M., Banari, A., Janssen, C.F., Shock, J.J. and M. Uberrueck. (2015) Solution of viscous flows in a hybrid naval hydrodynamic scheme based on an efficient Lattice Boltzmann Method. In *Proc. 13th Intl. Conf. on Fast Sea Transportation* (FAST 2015; Washington D.C., September 1-4, 2015).

O'Reilly C.M., Grilli S.T., Harris J.C., Mivehchi A., Janssen C.F. and J. Dahl 2016. Development of a hybrid LBM-potential flow model for Naval Hydrodynamics. In Proc. 15th Journe de l'hydrodynamique (JH2016) (November 22-24, Brest, France), 15pps.

Reliquet, G., A. Drouet, P.-E. Guillerm, L. Gentaz and P. Ferrant (2014). Simulation of wave-ship interaction in regular and irregular seas under viscous flow theory using the SWENSE method. In *Proc. 30th Symp. Naval Hydrod.* (Tasmania, 11/2014), 11 pps.